Thin Solid Films 799 (2024) 140399

Contents lists available at ScienceDirect

Thin Solid Films

journal homepage: www.elsevier.com/locate/tsf

Adhesive-free bonding for hetero-integration of InP based coupons micro-transfer printed on SiO_2 into Complementary Metal-Oxide-Semiconductor backend for Si photonics application on 8″ wafer platform

K. Anand [a,*], P. Steglich [a,b], J. Kreissl [a], C.A. Chavarin [a], D. Spirito [a], M. Franck [a], G. Lecci [a], I. Costina [a], N. Herfurth [a], J. Katzer [a], C. Mai [a], A. Becker [c], J.P. Reithmaier [c], L. Zimmermann [a,d], A. Mai [a,b]

[a] IHP-Leibniz-Institut für innovative Mikroelektronik, Im Technologiepark 25, 15236 Frankfurt (Oder), Germany
[b] Technische Hochschule Wildau, Hochschulring 1, 15745 Wildau, Germany
[c] Universität Kassel, Heinrich-Plett-Str. 40, 34132 Kassel, Germany
[d] Technische Universität Berlin, HFT-TA 315, Einsteinufer 25, 10587 Berlin, Germany

ARTICLE INFO

Keywords:
Hetero-integration
Micro-transfer printing
Indium Phosphide
Silicon Oxide
Sacrificial layer
Oxygen plasma activation

ABSTRACT

Micro-Transfer printing (μTP) is a promising technique for hetero-integration of III-V materials into Si-based photonic platforms. To enhance the print yield by increasing the adhesion between the III-V material and Si or SiO_2 surface, an adhesion promoter like Benzocyclobutene is typically used as interlayer. In this work, we demonstrate μTP of InP based coupons on SiO_2 interlayer without any adhesive interlayer and investigate the mechanism of adhesive free bonding. Source coupons are InP-based coupon stacks on a sacrificial layer that is removed by a chemical wet etch with $FeCl_3$. For the target we fabricated amorphous-Si waveguides on 8″ wafer encapsulated by a High Density Plasma SiO_2 which was planarized by a chemical mechanical polishing procedure. We used O_2 plasma to activate both source and target to increase adhesion between coupon and substrate. To get a better understanding of the bonding mechanism we applied several surface characterization methods. Root mean square roughness of InP and SiO_2 was measured by atomic force microscopy before and after plasma activation. The step height of the micro-transfer printed source coupon on the target wafer is estimated by optical step profiler. We used Raman peak position mappings of InP to analyze possible strain and contact angle measurements on SiO_2, before and after plasma activation to observe a change in the hydrophilicity of the surface. X-ray Photoelectron Spectroscopy analysis was used to characterize the surface energy states of P2p, In3d, O1s for InP source and Si2p, O1s for SiO_2 target. Our results demonstrate direct bonding of InP coupons by means of μTP without the need of a strain-compensation layer. In this way, a promising route towards Complementary Metal-Oxide-Semiconductor compatible use of μTP for the hetero-integration of InP is provided.

1. Introduction

Hetero-integration of Group III/V materials on Group IV has been extensively carried out in recent times for various devices such as lasers, photodiodes and light emitters [1] as well as in applications such as communication and sensing [2]. Various techniques for hetero-integration are reported, e.g. wafer bonding [3] and micro-transfer printing (μTP) [4]. μTP is advantageous over wafer bonding as it offers higher throughput, enables efficient material use, involves lower temperature and high-precision positioning of devices on substrate. However, these methods require adhesives such as Benzocyclobutene (BCB) [5] and SU-8 [6] as well as strain-compensation metal layers such as gold [7], which could be potential contaminations for the cleanroom while post-processing. They are also likely to make interconnects and hence are not very widely used. Additionally, the presence of extra adhesive/metal interlayer in between poses difficulty in evanescent light coupling from laser source to waveguide target. In previous works, the μTP approach has been used for hetero-integration

* Corresponding author.
E-mail address: anand@ihp-microelectronics.com (K. Anand).

https://doi.org/10.1016/j.tsf.2024.140399
Received 14 November 2023; Received in revised form 24 May 2024; Accepted 28 May 2024
Available online 29 May 2024

of Group III/V materials on Group IV both with use of adhesives such as BCB [8] and without [9]. In this work, we demonstrate a hetero-integration approach of InP on SiO_2 using μTP, without the use of any adhesives or without the need of any additional strain-compensation layer. Our approach is based on surface activation for both InP source and SiO_2 target using O_2 plasma and thereby realizing reduced residual strain in the InP layer by partial removal of surrounding photoresist by plasma treatment. We also investigate the mechanism of adhesive free bonding for hetero-integration of InP based coupons on SiO_2 interlayer by μTP, within Complementary Metal-Oxide-Semiconductor (CMOS) structure for application of III/V lasers into Electronic-Photonic Integrated Circuit technology.

2. Experimental

2.1. Source coupon preparation

Different sizes of coupons (400 μm x 50 μm, 800 μm x 50 μm and 1200 μm x 50 μm) processed from an InP-based coupon stack with sacrificial layer grown by a solid source molecular beam epitaxy on InP (100) substrate are fabricated as shown in layer stack schematics in Fig. 1. The 500 nm thick sacrificial layer was removed by wet etching in 27.5 % $FeCl_3$ for 100 min at 6 °C to expose the bottom layer of the coupon stack (InP) as the mating surface with the target. Cross-section images of the resist covered source coupon cut out by Focused Ion Beam (FIB), before and after under etching for sacrificial layer removal are shown in Fig. 2a and b. The purpose of resist is to protect the underlying III/V coupon stack during the micro-transfer printing process and is stripped later on during post-processing for laser fabrication.

2.2. Target wafer preparation

For the fabrication of the target wafer, we realized amorphous-Si (a-Si) waveguides embedded in SiO_2 stack. At first, a SiO_2 with a thickness of around 3 μm and an a-Si layer were deposited by a plasma enhanced chemical vapor deposition (CVD). Afterwards, waveguides were

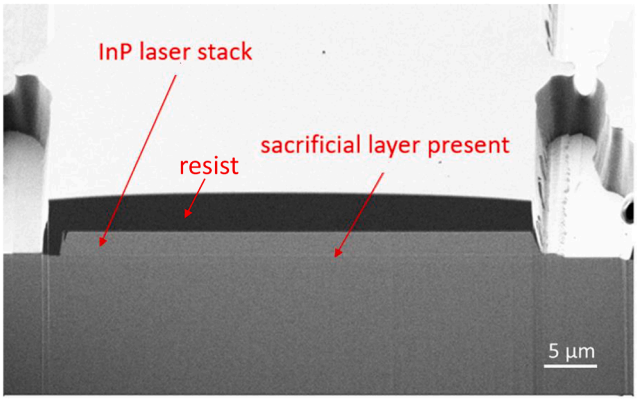

(a)

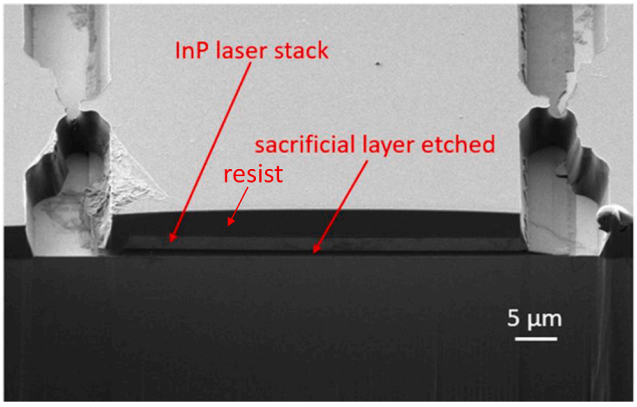

(b)

Fig. 2. Cross-section images of InP source coupon by FIB cut (a) before sacrificial layer under etching, (b) after sacrificial layer under etching. The resist acts as a protective layer to hold intact the InP coupon stack.

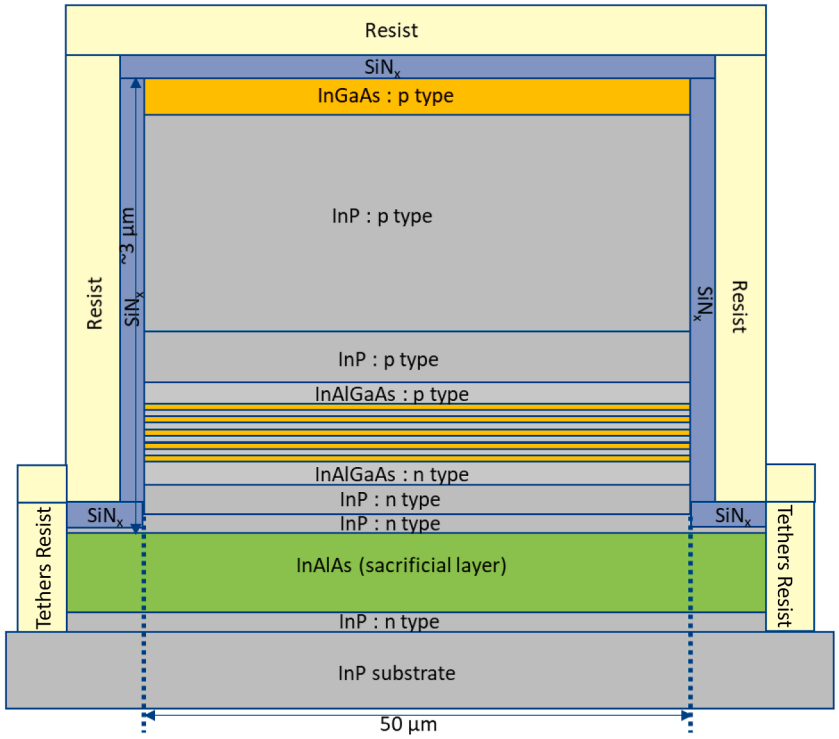

Fig. 1. Schematics of InP based coupon stack cut through the tethers with 500 nm thick sacrificial layer.

patterned by applying a deep ultraviolet 248 nm lithography followed by reactive ion etching (RIE). The mask utilized for the lithography procedure also contains alignment marks which are required for the μTP. The a-Si test structures were encapsulated by a SiO_2 deposited by high density plasma (HDP) CVD. Finally, the target wafer was planarized by a chemical mechanical polishing (CMP) procedure. As depicted in Fig. 3b, the distance between a-Si waveguides and SiO_2 surface was around 130 nm.

2.3. Oxygen plasma activation

For the activation of source and target wafer surface required for the μTP, we use the following Oxygen plasma conditions - Power: 50 W; Time: 100 s; Temperature: ~100 °C; Pressure: 33 Pa; O_2 flow: 35 sccm. The source coupon activation takes place as follows: Upon O_2 plasma treatment, the diffusion length of oxygen ions is sufficient enough to reach the under-etched backside of InP source coupon through the thick gaps formed by removal of 500 nm thick sacrificial layer and the native InP substrate. The reflection of oxygen ions incident at the InP substrate is the expected reason for surface activation of the coupon underside. For the target wafer, the plasma in contact with the surface breaks existing molecular bonds thereby incorporating polar functional groups which changes the surface termination and increases the surface energy resulting in improvement of adhesion and bonding. Oxygen plasma

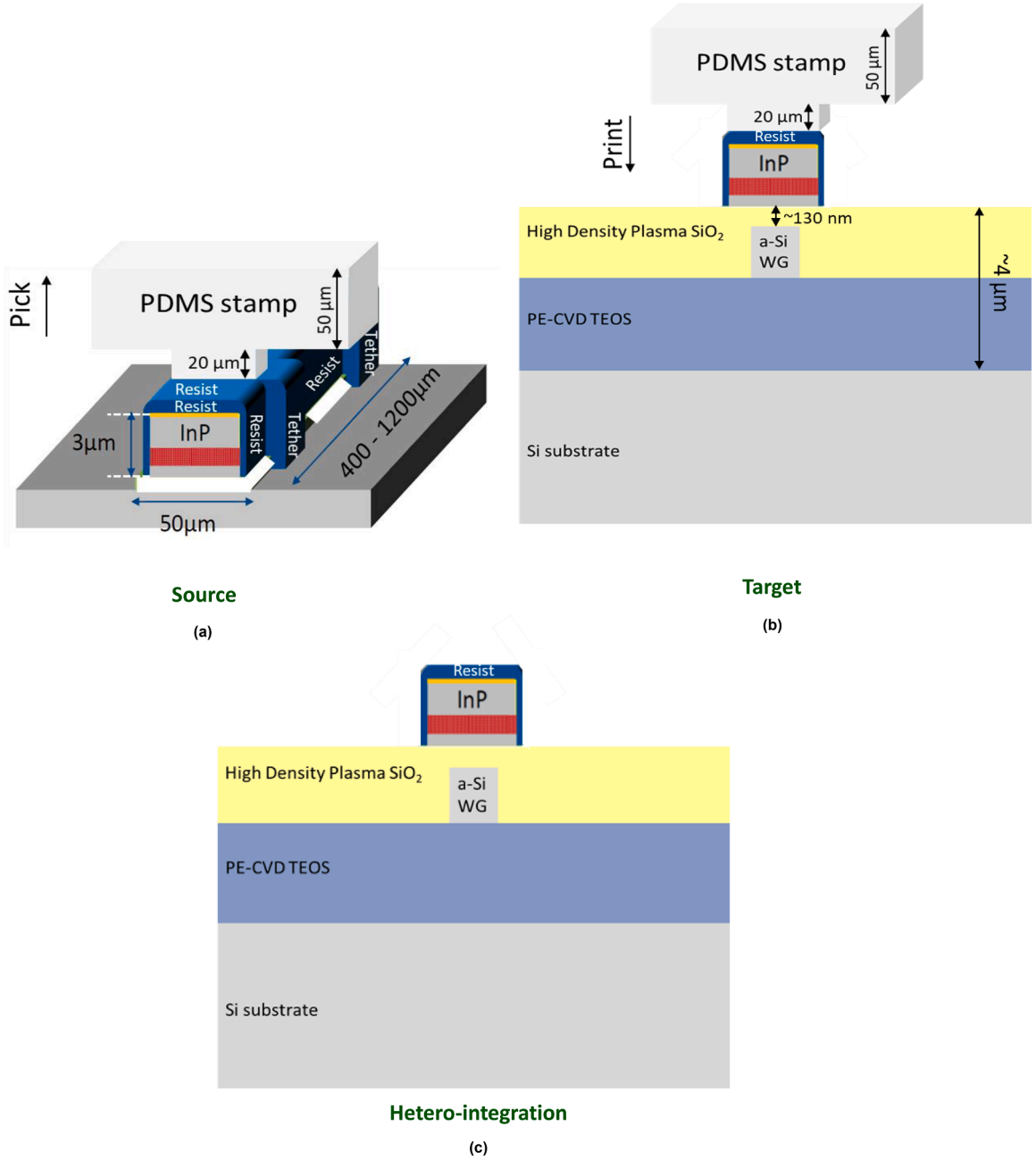

Fig. 3. μTP process flow schematics depicting (a) isometric view of under-etched InP source with resist covering. The source coupon is plasma activated such that the O_2 plasma reaches the under-side through the gaps formed after sacrificial layer removal. PDMS stamp with 20 μm thick post and 50 μm thick super-post is used for picking up the InP source coupon, (b) cross-sectional view of SiO_2 target with a-Si waveguides embedded ~130 nm deep inside the HDP SiO_2 surface. The target wafer is also plasma activated. The same PDMS stamp is used for printing down the InP coupon stack with resist covering, at right position just above the a-Si waveguides, (c) hetero-integration of InP source on SiO_2 target using hydrogen bridge bonding.

activation of both source and target is performed using Sentech SI 591 compact RIE Plasma tool.

2.4. μTP process

μTP of InP source on SiO_2 target is carried out with a X-Celeprint MTP-200 M tool. Both source and target wafers are placed in the tool chuck immediately after O_2 plasma activation. Then the under etched InP source coupon is picked up by a Poly Di-Methyl Siloxane (PDMS) stamp, and transfer printed at the right position on the SiO_2 target wafer. PDMS stamp with dimensions same as that of the InP coupon having 20 μm thick post and 50 μm thick super-post is used for picking up and printing down the InP source coupon covered with resist on SiO_2 target wafer. The process flow is shown in schematics as in Fig. 3a-c.

2.5. Characterization

We used various techniques for material characterization of the InP source coupon and SiO_2 target wafer. The InP coupon stack was picked up by double-sided carbon tape and flipped so that the InP underside was exposed for characterizations as shown in Fig. 4a and b. The plasma treatment was done after flipping the InP source coupon because otherwise it would be difficult to characterize the InP source coupon with plasma treatment prior to flipping since picking up successfully by double-sided tape, finding the coupons on the tape by optical microscope and characterizing by different techniques is altogether a time-taking and tricky process. Moreover, due to the fact that the plasma activation has time dependence (1 hour for SiO_2 target wafer) hence, this would mean we need to characterize the InP coupon which is already plasma activated on flipping, within 1 hour, which is very challenging. The results from the flipped InP samples for characterization can be transferred to the unaltered sample up to reasonable extent. There is no use of any sputtering ion beam species, beam energy and beam current density. X-ray Photoelectron Spectroscopy (XPS) measurements for the InP source were performed using a Ulvac-Phi VersaProbe II with pass energy 29.35 eV and energy steps of 0.125 eV, whereas for the SiO_2 target, a custom tool from SPECS GmbH was used, both utilizing Al-K_α X-ray sources with pass energy 20 eV and energy steps of 0.1 eV. It has been used to characterize the source and target, before and after O_2 plasma activation. The binding energy scale of the spectra has been referenced with respect to the standard C1s peak. The peak fit analysis was performed using CASAXPS peak fitting software.

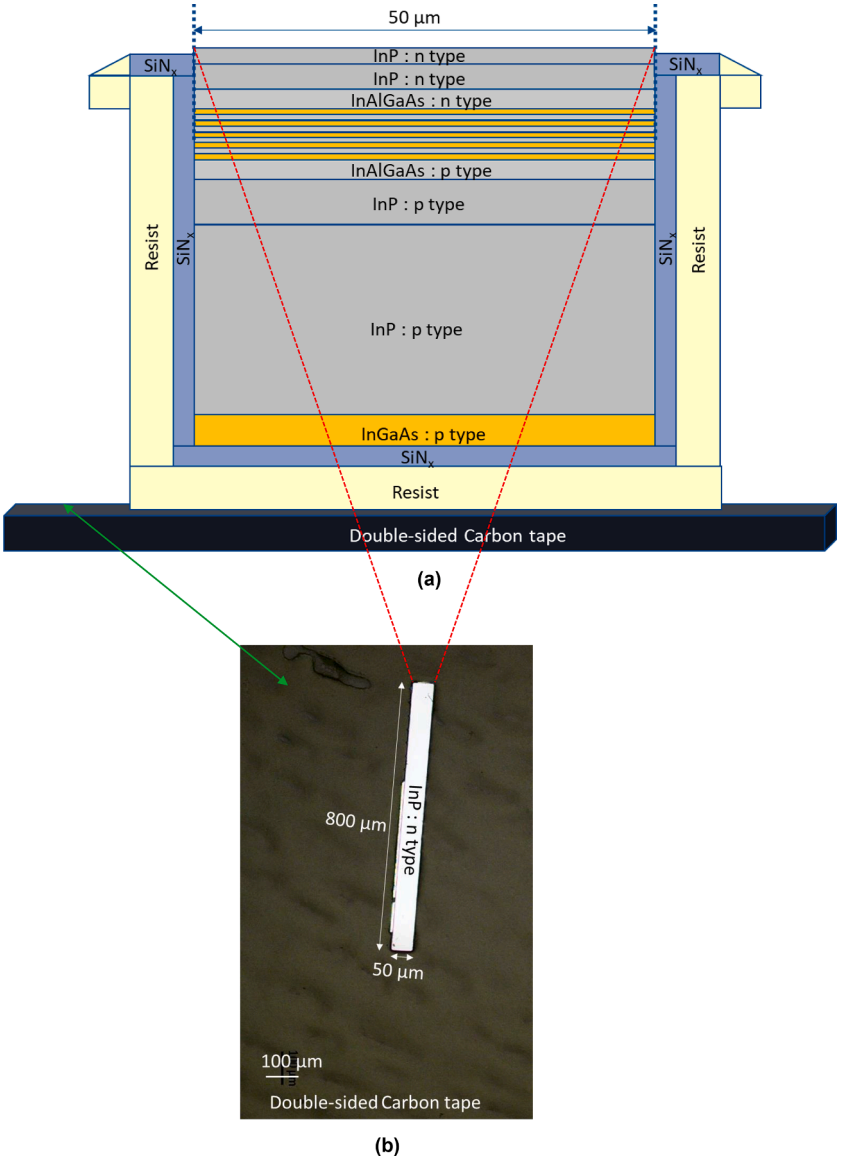

Fig. 4. Source coupon preparation for characterization (a) schematics of flipped InP source by double-sided carbon tape, (b) optical image of exposed InP under side.

The peak fitting was done in Tougaard background with Gaussian-Lorentzian line shapes. For the peak fit analysis, the fitting parameters were constrained as follows: Same Full Width Half Maximum for the two peaks of the doublet (for ex. In $3d_{3/2}$ and In $3d_{5/2}$; P $2p_{1/2}$ and P $2p_{3/2}$ etc.), ratio of area of peaks for In $3d_{3/2}$ and In $3d_{5/2}$ is 2:3 and that for P $2p_{1/2}$ and P $2p_{3/2}$ is 1:2. Peak position was not constrained, but it matched the literature value of spin-orbit splitting. Atomic Force Microscopy (AFM) measurements were done using a neaSNOM system from NEASPEC in non-contact AFM mode with metal-coated Si tips with a nominal resonance frequency of 75 kHz (Multi75E-G). It has been used to measure the surface roughness of the InP source coupon surface (after sacrificial layer removal) and SiO_2 target surface, before and after O_2 plasma activation. Micro-Raman spectroscopy was measured by excitation with a 532 nm laser focused on the sample with spot size ~1 μm. Scattered light was analyzed with a 3000 lines/mm grating. Contact angle measurement is done to examine the difference in surface energy of SiO_2 surface, before and after O_2 plasma activation. An optical step profiler is used for estimating the step height and bending at the surface and/or interface of micro-transfer printed source coupon on target wafer.

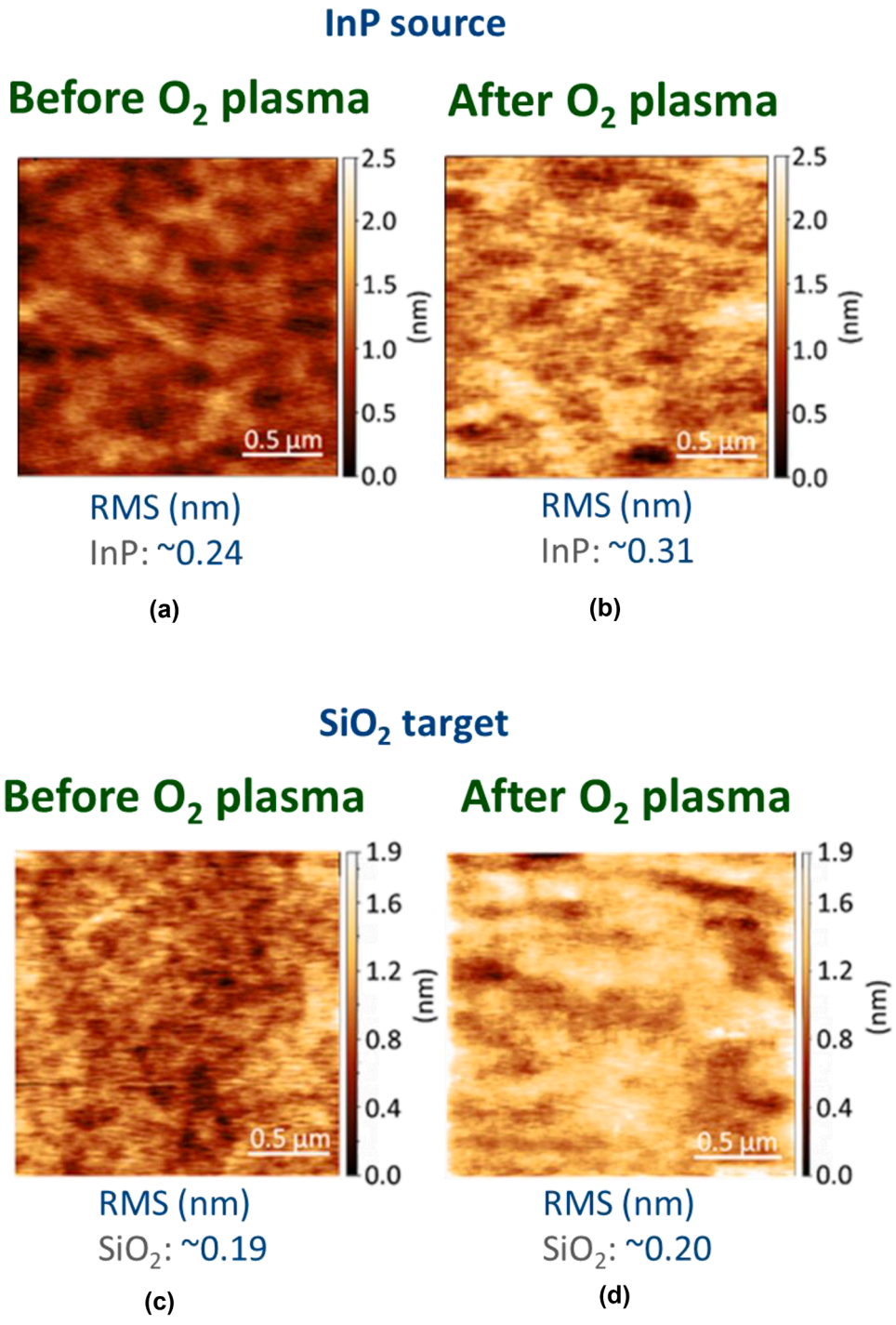

Fig. 5. AFM surface topography image of InP under side (a) before plasma activation, (b) after plasma activation. AFM surface topography image of SiO_2 target (c) before plasma activation, (d) after plasma activation.

3. Results and discussion

3.1. Roughness measurements

Fig. 5a and b show the AFM surface topography images of the InP underside surface, before and after O_2 plasma activation. For a scan size of 2 μm x 2 μm, the root mean square (RMS) of the surface of the InP underside before plasma treatment is ~0.24 nm whereas after plasma it is ~0.31 nm. Although the surface roughness measurements were done on the underside of the same InP coupon, but the area of analysis (2 μm x 2 μm) cannot be exactly the same before and after plasma activation hence, there is a standard deviation for the roughness values which is within the variation of roughness over the sample. The under etching by $FeCl_3$ is uniform and exposes a smooth InP surface.

The AFM topography images of the SiO_2 surface, before and after O_2 plasma activation is shown in Fig. 5c and d. Scan size of the sample is 2 μm x 2 μm. The RMS of the SiO_2 surface before plasma is ~0.19 nm whereas after plasma it is ~0.20 nm. The CMP of the grown oxide helps to achieve a smooth surface, with roughness in the sub-nanometer range. Also, the plasma activation has no significant effect on the surface roughness of the target substrate.

3.2. Optical step-profile: InP on SiO_2

Fig. 6a and b show the step height of a micro-transfer printed InP source covered by resist on SiO_2 target measured by an optical step profiler using an infra-red laser, with line scans averaged along horizontal length and along vertical width respectively. The features that appears on the surface of the transferred coupon are due to the ashing effect from Oxygen plasma treatment on resist. This doesn't affect the underlying InP coupon stack since it is protected by thick resist. We find that the average step height of the coupon is ~4.55 μm after several scans, both along width and length. This indicates that the source coupon is printed very flat onto the target and there is no significant bending or lift off of the coupons at the surface and/or interface, after printing.

3.3. Micro-Raman: InP source

Fig. 7 reports the results of Micro-Raman spectroscopy. The strongest feature is the longitudinal optical mode of InP, that is observed in the range 340–350 cm^{-1}, and that is sensitive to strain of the layer [10].

Measurements are performed on an InP source coupon (800 μm x 50 μm), near the edge and in the interior of the coupon, before and after plasma treatment. Fig. 7a displays exemplary spectra.

Before plasma treatment, in the center of the coupon, a peak is found around 344 cm^{-1}, which matches with unstrained InP [10]. At the edge, a shoulder is observed at this energy, with a stronger peak at 349 cm^{-1}, corresponding to a compressive strain of −0.7 % (considering a strain-shift coefficient of −660 cm^{-1} [11]). After plasma treatment, the peak shifts to the unstrained case at the edge, and possibly indicates a slightly tensile strain at the center (+0.3 %). In general, both before and after plasma treatment, the Raman peak in the internal part of the coupon is at lower energy than at the edge.

Spatial distribution of the peak energy is displayed in Fig. 7b. Both before and after plasma, the center is rather uniform. Before plasma treatment, the external part (around 25 μm from the corner of the coupon) stands out with the stronger peak at higher energy, corresponding to compressive strain as discussed before. After plasma the difference between interior and periphery is much reduced, with a reduction of the energy on the whole coupon.

These results can be explained as follows: There can be strain from SiN_x, resist and material. But the possibility of strain from SiN_x passivation layer is the highest because it is in direct contact with the material. Regarding the strain from the material, it is unlikely because the III/V coupon stack is epitaxially grown lattice-matched [12] and all the layers are equally strained everywhere. However, there are chances of strain from the SiN_x because of difference in thermal expansion coefficient between SiN_x and InP: since SiN_x has higher thermal expansion coefficient than InP, hence during cooling after SiN_x deposition, it contracts more than InP thereby inducing compressive strain (higher Raman peak positions) at the edges of InP coupon as compared to that at the center. After plasma activation (at ~100 °C), due to the ashing of some surrounding resist material capping the SiN_x passivation layer on InP, the resist thickness on SiN_x is reduced which leads to decrease in compressive strain (relaxation) at the edge. The edge is especially affected by the combination of photoresist and SiN_x. These findings highlight the sensitivity of the membrane to surrounding layers (SiN_x and resist). The strain relaxation effect after plasma treatment is beneficial since it will minimize the bending effect caused by induced residual strain in the InP

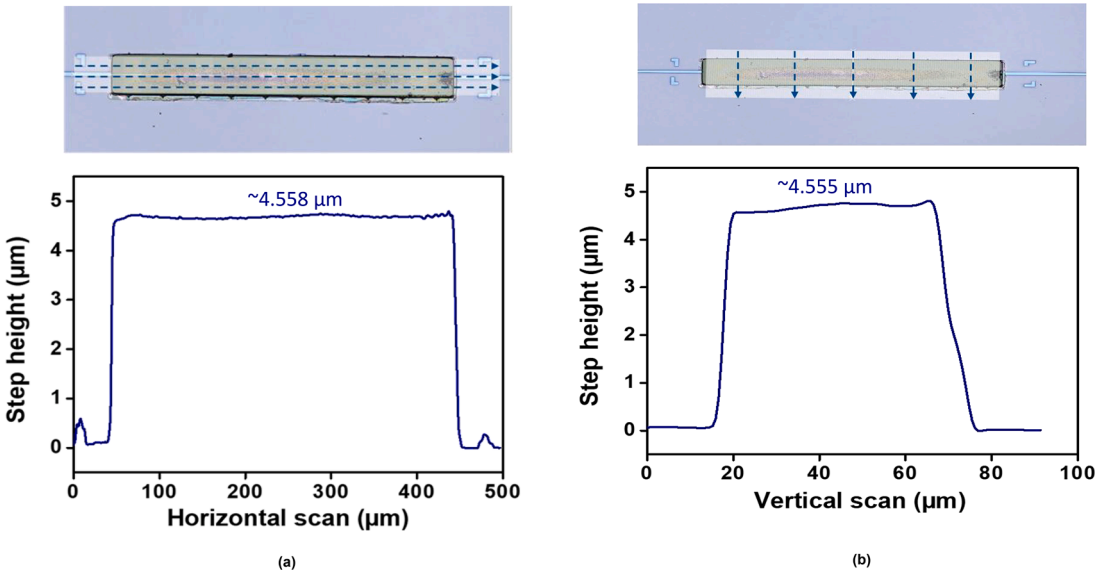

Fig. 6. Step-height of InP coupon stack covered with resist which is micro-transfer printed on SiO_2 target measured by optical step profiler. The light blue box on the InP coupon stack with resist on top denotes the numerous line scans along the scanning directions depicted by dotted arrows. These line scans are averaged along (a) horizontal directions from left to right, (b) vertical directions from top to bottom.

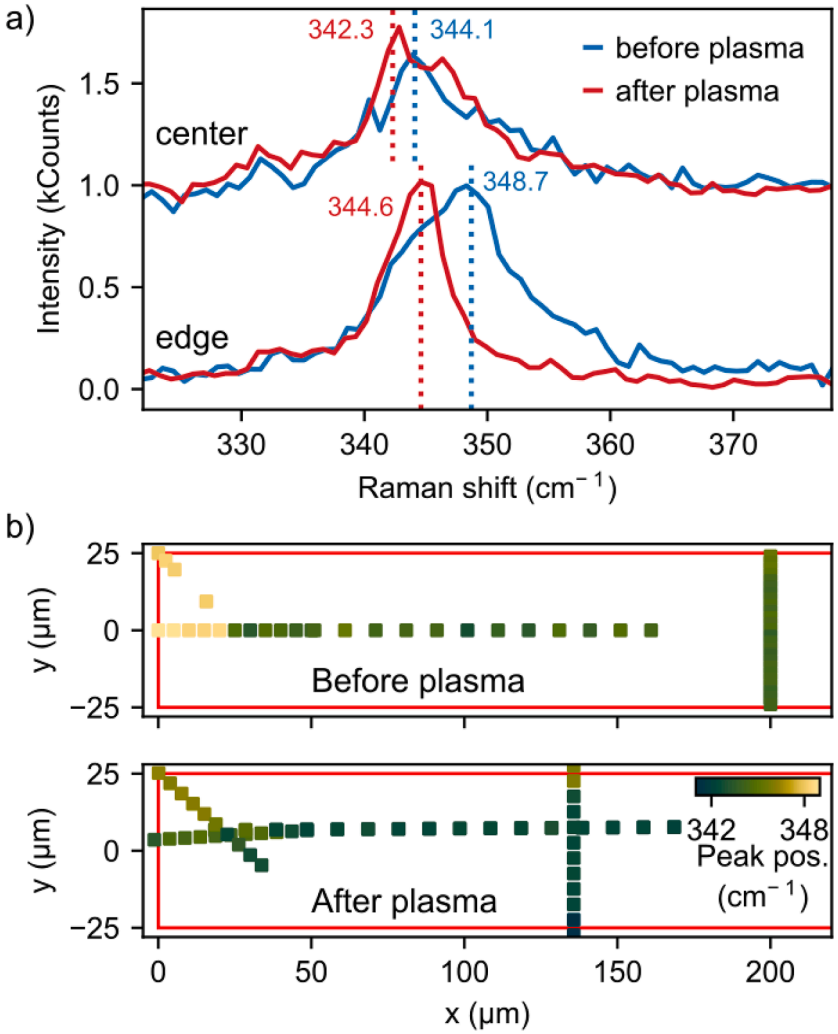

Fig. 7. (a) Raman spectra of InP source at center and edge, before and after plasma. Curves are vertically offset for clarity. Dotted lines mark the peak position. (b) Maps of the Raman peak position from InP source before plasma and after plasma. Red solid lines mark the edges of the coupon. Color scale is the same in both panels.

source coupon, which in turn is advantageous for hetero-integration by micro-transfer printing.

3.4. Contact angle: SiO_2 target

Contact angle measurements with de-ionized water drops on SiO_2 wafer at three different positions are done. The mean contact angle obtained is 82.8°±0.04° before plasma treatment whereas it is 22.6° ±0.03° after plasma treatment. The contact angle measurement reveals a significant reduction in the mean contact angle of water drop which implies that hydrophilicity increases after oxygen plasma. This indicates that there is an increase in surface energy of the SiO_2 surface after plasma activation, which helps improving subsequent adhesion and bonding.

3.5. XPS

3.5.1. InP source

Fig. 8a shows the P 2p XPS spectra for the InP source coupon before and after O_2 plasma activation, respectively. The black curve represents the raw data, which is fitted (gray) and deconvoluted into several components: The peaks at 127.1 eV (red) and 127.9 eV (blue) are attributed to the $2p_{3/2}$ and $2p_{1/2}$ components of the P-In bonds from InP, while the peaks at 132.2 eV (green) and 133.2 eV (magenta) belong to the corresponding P-O bonds from $InPO_x$ [13,14]. The surface of the InP source coupon is clearly oxidized through exposure to ambient air after etching of the sacrificial layer. After plasma treatment, these peaks exhibit only a minimal shift of $\Delta = \pm 0.1$ eV. We find that an additional satellite peak at binding energy 124.7 eV (dark yellow) appears only after plasma activation. The precise origin of this peak is unclear at the moment, but it is speculated to correspond to the below mentioned additional peak at 533.4 eV observed in the O 1s spectrum (of InP source) after plasma treatment. However, the lower binding energy position is counterintuitive, as oxidation-related peaks are expected at higher binding energies compared to the unoxidized InP state, due to the high electronegativity of oxygen. A lower binding energy could indicate a lower electronegativity bonding partner than In, which is highly unlikely in our case. Consequently, further investigation is needed to clarify the peak origin.

The In 3d XPS spectra for the InP source coupon before and after O_2 plasma activation are shown in Fig. 8b, respectively. The black curve represents the raw data, which is fitted (gray) and deconvoluted into multiple components: The peaks at 442.9 eV (red), 443.1 eV (dark yellow) and 444 eV (blue) are attributed to the $3d_{5/2}$ component of the In-P bonds from InP, In-O bonds from In_2O_3 and In-$(PO_x)^{3-}$ bonds from $InPO_x$, respectively. The corresponding $3d_{3/2}$ components are found at 450.4 eV (green), 450.7 eV (navy) and 451.6 eV (magenta), respectively [13,15,16,17,18]. Both $3d_{5/2}$ and $3d_{3/2}$ peaks are only minimally shifted

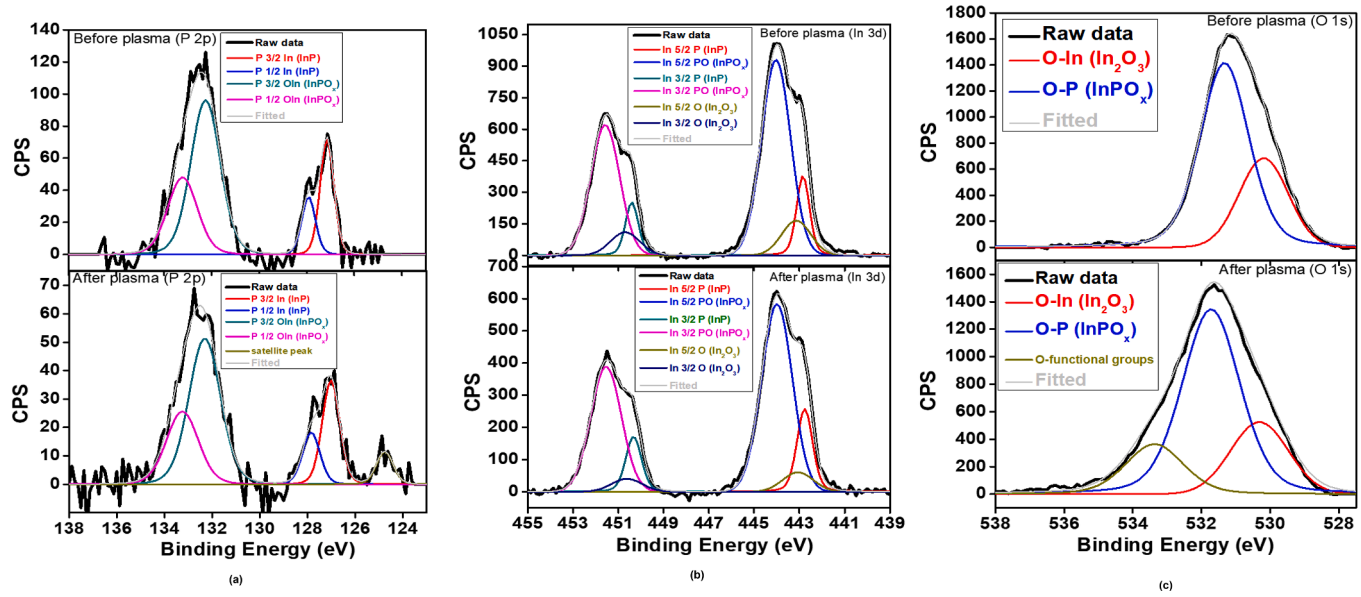

Fig. 8. XPS analysis of InP source coupon (a) P 2p peaks before plasma activation and after plasma activation, (b) In 3d peaks before plasma activation and after plasma activation, (c) O 1s peaks before plasma activation and after plasma activation. The before plasma activated and after plasma activated spectra for all, is vertically placed to each other for direct comparison.

by −0.1 eV after plasma activation. Notably, no additional peaks appear after plasma activation, indicating that oxygen plasma does not react with In to form any new species.

Fig. 8c depict the O 1s XPS spectra for the InP source coupon before and after O_2 plasma activation, respectively. The black curve represents the raw data, which is fitted (gray) and deconvoluted into the following components: A peak at 531.3 eV, attributed to O-P bonds from $InPO_x$ (blue) and one at 530.2 eV, attributed to O-In bonds from In_2O_3 (red) [13]. After plasma treatment, the O-P and O-In peaks are shifted by $\Delta =$ 0.4 eV and $\Delta = 0.1$ eV, respectively. Moreover, we find that an additional peak at binding energy 533.4 eV (dark yellow) appears only after plasma activation. This is possibly because the oxygen plasma diffusion length is sufficient to reach the exposed InP surface underneath through the gap formed after sacrificial layer removal, thereby breaking existing molecular bonds and incorporating oxygen-containing functional groups. The surface energy is increased, which improves adhesion and bonding.

3.5.2. *SiO_2 target*

Fig. 9a show the Si 2p XPS spectra of the SiO_2 target wafer, before and after O_2 plasma activation, respectively. The black curve represents the raw data, which is fitted (gray) and deconvoluted into the following components: The peaks at 103.0 eV (red) and 104.6 eV (blue) are attributed to Si-O bonds from SiO_2 and SiO_4, respectively [19]. The plasma activation introduced a minimal shift of 0.1 eV for both peaks. We find that an additional peak at binding energy 106.6 eV (green) appears only after activation. This additional peak at higher binding energy may originate from the introduction of new oxygen-containing functional groups and vacancies after plasma treatment which acts as additional activated sites and thereby increasing the surface energy and enhancing adhesion and bonding.

The corresponding O 1s XPS spectra of the SiO_2 target wafer before and after O_2 plasma activation are shown in Fig. 9b, respectively. The black curve represents the raw data, which is fitted (gray) and deconvoluted into the following components: The SiO_2 peak (red) appears at 531.8 eV, while the peak at 533.3 eV (blue) is attributed to an even higher oxidation state, SiO_4 [19]. After plasma treatment, these peaks were shifted by ±0.1 eV. Furthermore, an additional peak is found at 535.9 eV (green) only after plasma treatment, which corresponds to the aforementioned oxygen containing functional groups.

Fig. 9c shows the time dependent variation of the higher binding energy peak at ~536 eV in the O 1s spectrum of the SiO_2 target wafer. This peak is reduced in intensity compared to the peak at ~532 eV over time. The ratio of intensities $I_o = I_{536\ eV}/I_{532\ eV}$ varies as follows: 2.38 within 1 hour of plasma activation; 0.38 after 3 h of plasma activation and 0.30 after 24 h of plasma activation, as shown in the inset of Fig. 9c. It is interesting to note that after about 1 h time, we need to re-activate the target wafer for successful μTP. This indicates $I_o > 2$ as a rule of thumb for a good process window. This technique of adhesive-less printing by plasma activation of source and target is a CMOS compatible route of hetero-integration without any adhesive or strain-compensation layer.

3.6. *Shear parameters: InP on SiO_2*

After printing is done, the target wafer shears off from the stamp with a certain speed and up to a certain distance in X-Y for a set duration, which is referred to as shear speed and X-Y shear distances respectively. The bond strength is sufficient such that the printed coupon is stable after further post processing steps on other tools, like ashing for complete removal of resist followed by HDP SiO_2 deposition and CMP. Additionally, the adhesive force of printed source on target is strong enough as it can withstand minor mechanical vibrations during transport of the printed wafers to another lab in a different city for post-processing steps. The critical shear speed of the target is 600 μm/*sec* which is crucial as a qualitative method in determining the stability of the printed coupons. This was obtained by varying the shear speed parameter in the MTP tool. Also, increasing the shear distance reduces pull-off force for delaminating the stamp from the target (Y shear distance increased from 60 μm to 120 μm) [20]. There were around 250 coupons printed out of 275 coupons with ~90 % local yield. By local yield, it is meant that the printing was done in several attempts on different substrates using different coupons over the period of time. Fig. 10a and c show optical images of many such printed coupons. The magnified image of one of the printed coupons from Fig. 10a is shown in Fig. 10b. In Fig. 10a, we see that all 4 coupons of size 800 × 50 μm are printed whereas in Fig. 10c, we see that 3 coupons of size 800 × 50 μm are printed and 2 coupons of size 400 × 50 μm (only half as long) are

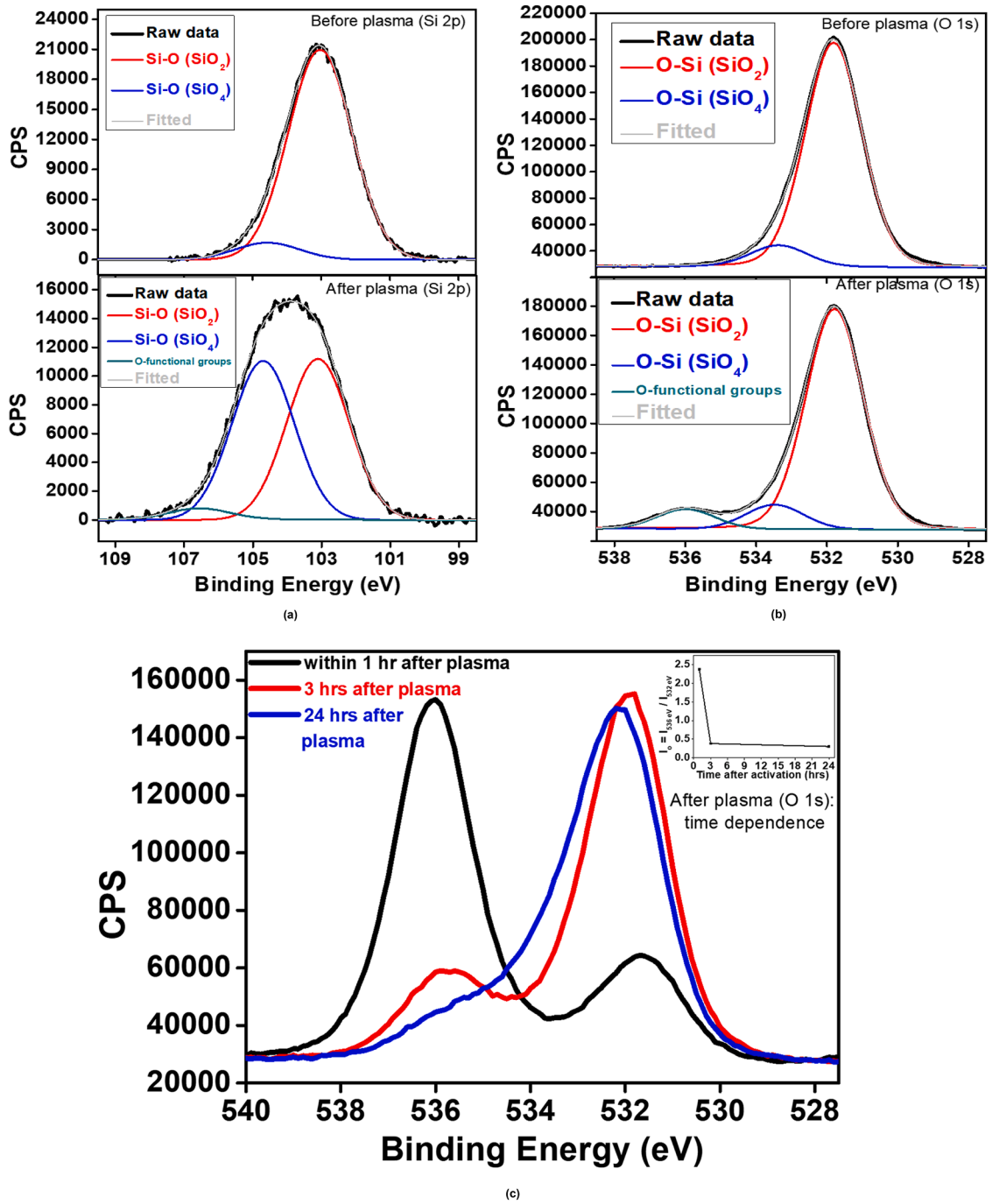

Fig. 9. XPS analysis of SiO_2 target wafer (a) Si 2p peaks before plasma activation and after plasma activation, (b) O 1s peaks before plasma activation and after plasma activation, (c) Time dependence variation of $I_{536\ eV\ peak}$ from O 1s spectra of SiO_2 target wafer after plasma activation.

printed. All the coupons are covered with resist and no coupons are broken or delaminated. The residues left on the device are from the resist after plasma activation. This resist is just used as a protection layer on top of the laser stack. After the laser stack is transferred, there is ashing process for resist removal. Then HDP SiO_2 is deposited followed by CMP to form InP laser stack encapsulated in oxide. The transfer-printing method here is just an intermediate step after which there are several post-processing steps involved for laser fabrication.

4. Conclusion

Hetero-integration of InP on SiO_2 by means of direct-bonding with μTP is demonstrated. The aim of the adhesive-free technique is to fulfill all the requirements of CMOS compatibility hence, we don't use BCB or other adhesive materials. Both source coupon and target wafer are activated by oxygen plasma. The RMS roughness of the InP and SiO_2 surfaces is in the range of ~0.2–0.3 nm, which is in the permissible limit of smooth roughness required for μTP. The InP source has a higher compressive strain at the edge as compared to the center before plasma treatment. This is because the InP membrane with SiN_x and photoresist deflects under residual strain at the edge. The decrease of residual strain after plasma activation at 100 °C could possibly be due to partial removal of the surrounding photoresist by oxygen plasma treatment. A uniform step height of ~4.55 μm is obtained by scanning average line scans both along horizontal and vertical directions which indicates no significant bending at the surface and/or interface. Further, contact

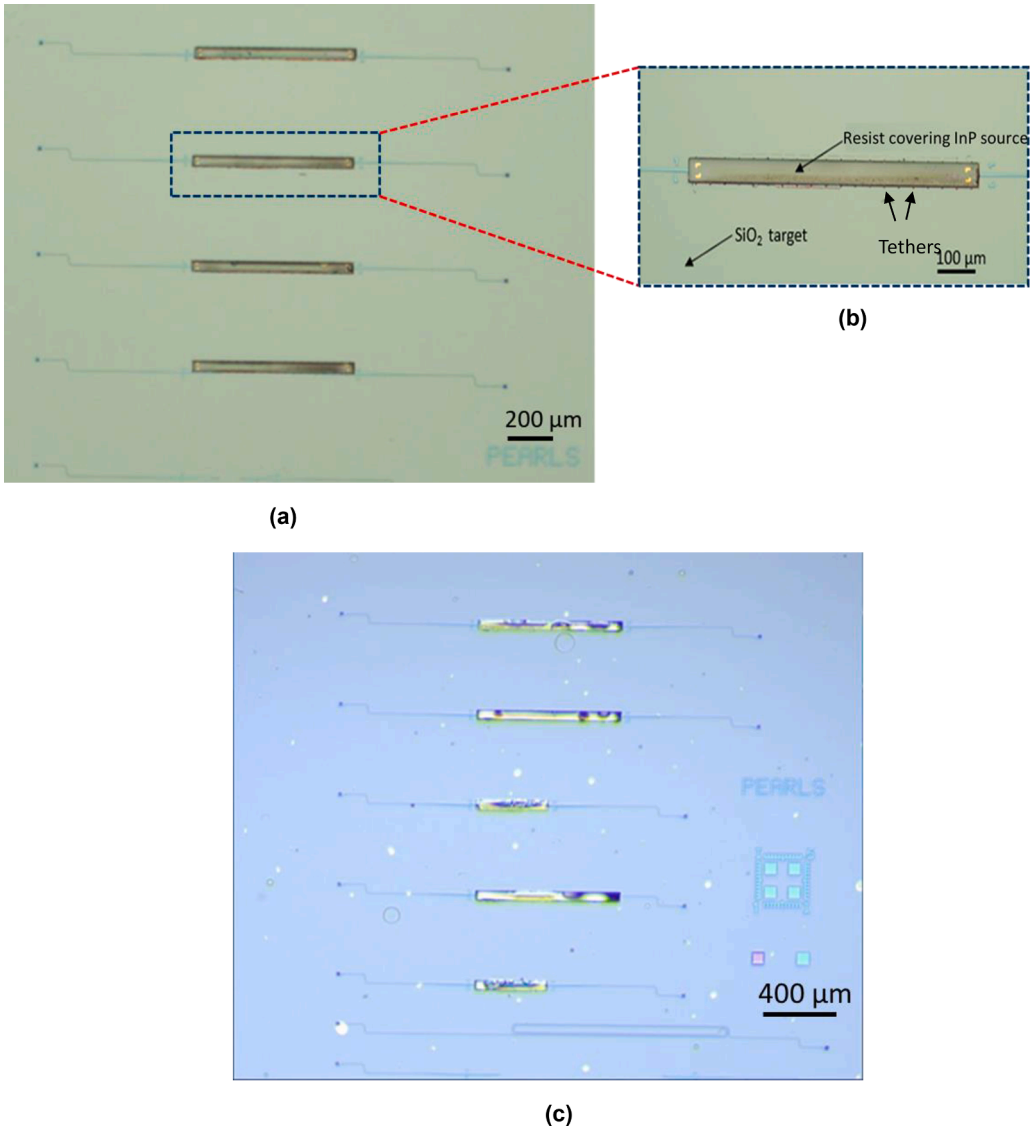

Fig. 10. Optical images of many such printed InP coupons (covered with resist) on SiO_2 target (a) all 4 printed coupons are of size 800 µm x 50 µm in one test field of SiO_2 target wafer with embedded a-Si waveguides, (b) magnified image of one such coupon for clear visibility, with resist covering on InP source and many tethers (like dots) along the printed coupon lengths, (c) 3 coupons of size 800 µm x 50 µm and 2 coupons of size 400 µm x 50 µm are printed in another test field of SiO_2 target wafer with embedded a-Si waveguides.

angle measurement of the SiO_2 target reveals that the mean contact angle reduces significantly after plasma treatment, thereby indicating an increase in surface energy which enhances adhesion/bonding. We observed additional peaks at higher binding energy in the O1s XPS spectra for both source (InP) and target (SiO_2). This indicates that the plasma treatment forms oxygen-containing functional groups/vacancies, which increases the surface energy thereby improving adhesion/bonding between the surfaces by hydrogen bridge bonds. The O_2 plasma surface activation leads to formation of broken dangling bonds on surface of SiO_2 and InP making the surface hydrophilic (Si-OH and InP-OH respectively) which reacts instantly with H_2O molecules from the air humidity. At room temperature, the adhesion between the two surfaces are via the monolayers of H_2O molecules and polar -OH terminations from SiO_2 and InP by hydrogen bonds [16]. Also, the plasma activation shows time-dependent variation hence a good process window for printing is guaranteed at least up to 1 hour after plasma activation. The printed source can withstand minor mechanical vibrations and is stable up to 600 µm/*sec* critical shear speed of target. These results define a methodology to characterize both the source coupons which are picked and target surface on which it is printed by µTP. Additional investigation of various parameters that are crucial for the printing process without adhesives is possible with the presented methodology. This technique opens a route towards CMOS-compatible hetero--integration of InP coupon stacks on SiO_2 without adhesives by µTP.

Funding

This research was supported by the BMBF projects (PEARLS, grant number 13N14936 and FMD, grant number 16FMD03).

CRediT authorship contribution statement

K. Anand: Conceptualization, Investigation, Formal analysis, Writing – original draft, Visualization. **P. Steglich:** Writing – review & editing, Validation, Methodology, Conceptualization. **J. Kreissl:** Writing – review & editing, Resources, Project administration, Conceptualization. **C.A. Chavarin:** Investigation, Formal analysis, Data curation. **D. Spirito:** Writing – review & editing, Investigation, Formal analysis, Data curation. **M. Franck:** Writing – review & editing, Investigation, Formal analysis, Data curation. **G. Lecci:** Writing – review &

editing, Resources, Methodology. **I. Costina:** Validation, Investigation, Formal analysis. **N. Herfurth:** Writing – review & editing, Investigation, Formal analysis, Data curation. **J. Katzer:** Investigation, Formal analysis. **C. Mai:** Resources, Investigation, Formal analysis, Writing – review & editing. **A. Becker:** Writing – review & editing, Resources, Methodology. **J.P. Reithmaier:** Resources, Methodology. **L. Zimmermann:** Writing – review & editing, Supervision, Funding acquisition. **A. Mai:** Writing – review & editing, Supervision, Funding acquisition.

Declaration of competing interest

The authors declare that they have no known competing financial interests or personal relationships that could have appeared to influence the work reported in this paper.

Data availability

Data will be made available on request.

References

[1] A.D. Groote, P. Cardile, A.Z. Subramanian, A.M. Fecioru, C. Bower, D. Delbeke, R. Baets, G. Roelkens, Transfer-printing-based integration of single-mode waveguide-coupled III-V-on-silicon broadband light emitters, Opt. Express 24 (2016) 13754–13762, https://doi.org/10.1364/OE.24.013754.

[2] G. Roelkens, A. Abassi, P. Cardile, U. Dave, A.D. Groote, Y.D. Koninck, S. Dhoore, X. Fu, A. Gassenq, N. Hattasan, Q. Huang, S. Kumari, S. Keyvaninia, B. Kuyken, L. Li, P. Mechet, M. Muneeb, D. Sanchez, H. Shao, T. Spuesens, A.Z. Subramanian, S. Uvin, M. Tassaert, K. Van Gasse, J. Verbist, R. Wang, Z. Wang, J. Zhang, J. Van Campenhout, X. Yin, J. Bauwelinck, G. Morthier, R. Baets, D. Van Thourhout, III-V-on-silicon photonic devices for optical communication and sensing, Photonics 3 (2015) 969–1004, https://doi.org/10.3390/photonics2030969.

[3] D. Caimi, P. Tiwari, M. Sousa, K.E. Moselund, C.B. Zota, Heterogeneous integration of III-V materials by direct wafer bonding for high-performance electronics and optoelectronics, IEEE Trans. Electron. Dev. 68 (2021) 3149–3156, https://doi.org/10.1109/TED.2021.3067273.

[4] J. Yoon, S.-M. Lee, D. Kang, M.A. Meitl, C.A. Bower, J.A. Rogers, Heterogeneously integrated optoelectronic devices enabled by micro-transfer printing, Adv. Opt. Mater. 3 (2015) 1313–1335, https://doi.org/10.1002/adom.201500365.

[5] S. Keyvaninia, M. Muneeb, S. Stankovic, P.J. Van Veldhoven, D. Van Thourhout, G. Roelkens, Ultra-thin DVS-BCB adhesive bonding of III-V wafers, dies and multiple dies to a patterned silicon-on-insulator substrate, Opt. Mater. Express 3 (2013) 35–46, https://doi.org/10.1364/OME.3.000035.

[6] F.J. Blanco, M. Agirregabiria, J. Garcia, J. Berganzo, M. Tijero, M.T. Arroyo, J. M. Ruano, I. Aramburu, K. Mayora, Novel three-dimensional embedded SU-8 microchannels fabricated using a low temperature full wafer adhesive bonding, J. Micromech. Microeng. 14 (2004) 1047–1056, https://doi.org/10.1088/0960-1317/14/7/027.

[7] R. Loi, S. Iadanza, B. Roycroft, J. O'Callaghan, L. Liu, K. Thomas, A. Gocalinska, E. Pelucchi, A. Farrell, S. Kelleher, R.F. Gul, A.J. Trinidade, D. Gomez, L. O'Faolain, B. Corbett, Edge-coupling of O-Band InP etched-facet lasers to polymer waveguides on SOI by micro-transfer-printing, J. Quant. Electron. 56 (2020) 6400108, https://doi.org/10.1109/JQE.2019.2958365.

[8] J. Zhang, G. Muliuk, J. Juvert, S. Kumari, J. Goyvaerts, B. Haq, C. Op de Beeck, B. Kuyken, G. Morthier, D. Van Thourhout, R. Baets, G. Lepage, P. Verheyen, J. Van Campenhout, A. Gocalinska, J. O'Callaghan, E. Pelucchi, K. Thomas, B. Corbett, A. J. Trindade, G. Roelkens, III-V-on-Si photonic integrated circuits realized using micro-transfer printing, APL Photon. 4 (2019) 110803, https://doi.org/10.1063/1.5120004.

[9] R. Loi, Heterogeneous Integration of InP Etched Facet Lasers to Silicon Photonics by Micro Transfer Printing, University College Cork, 2019. PhD thesis, https://hdl.handle.net/10468/8562.

[10] J. Arokiaraj, S. Tripathy, S. Vicknesh, A. Ramam, Realization of freestanding InP membranes on Si by low-temperature wafer bonding and stress analysis using micro-Raman spectroscopy, Appl. Phys. Lett. 88 (2006) 221901, https://doi.org/10.1063/1.2207834.

[11] S. Gennari, P.P. Lottici, F. Riccò, A Raman study of the strain in InP/GaAs heterostructures grown by MOVPE, Superlattices Microstruct. 17 (1995) 107–110, https://doi.org/10.1006/spmi.1995.1021.

[12] S. Mokkapati, C. Jagdish, III-V compound SC for optoelectronic devices, Mater. Today 12 (2009) 22–32, https://doi.org/10.1016/S1369-7021(09)70110-5.

[13] D.A. Granada-Ramirez, J.S. Arias-Cerón, M.L. Gómez-Herrera, J.P. Luna-Arias, M. Pérez-González, S.A. Tomás, P. Rodríguez-Fragoso, J.G. Mendoza-Alvarez, Effect of the indium myristate precursor concentration on the structural, optical, chemical surface, and electronic properties of InP quantum dots passivated with ZnS, J. Mater. Sci. Mater. Electron. 30 (2019) 4885–4894, https://doi.org/10.1007/s10854-019-00783-6.

[14] L. Xi, D-Y Cho, A. Besmehn, M. Duchamp, D. Grützmacher, Y.M. Lam, B. E. Kardynal, Effect of zinc incorporation on the performance of red light emitting InP core nanocrystals, Inorg. Chem. 55 (2016) 8381–8386, https://doi.org/10.1021/acs.inorgchem.6b00747.

[15] S.H. Kim, S.Y. Joo, H.S. Jin, W.-B. Kim, T.J. Park, Ultrathin ZnS and ZnO interfacial passivation layers for atomic-layer-deposited HfO_2 films on InP substrates, ACS Appl. Mater. Interfaces 8 (2016) 20880–20884, https://doi.org/10.1021/acsami.6b06643.

[16] J. Lin, T. You, T. Jin, H. Liang, W. Wan, H. Huang, M. Zhou, F. Mu, Y. Yan, K. Huang, X. Zhao, J. Zhang, S. Wang, P. Gao, X. Ou, Wafer-scale heterogeneous integration InP on trenched Si with a bubble-free interface, APL Mater. 8 (2020) 051110, https://doi.org/10.1063/5.0004427.

[17] K. Gong, C. Sun, B. Xiong, Y. Han, Z. Hao, J. Wang, L. Wang, H. Li, Oxides formation on hydrophilic bonding interface in plasma-assisted InP/Al_2O_3/SOI direct wafer bonding, AIP Adv. 7 (2017) 015039, https://doi.org/10.1063/1.4975345.

[18] T. Matsumae, R. Takigawa, Y. Kurashima, H. Takegi, E. Higurashi, Low-temperature direct bonding of InP and diamond substrates under atmospheric conditions, Sci. Rep. 11 (2021) 11109, https://doi.org/10.1038/s41598-021-90634-4.

[19] A.U. Alam, M.M.R. Howlader, M.J. Deen, Oxygen plasma and humidity dependent surface analysis of silicon, silicon dioxide and glass for direct wafer bonding, ECS J. Solid State Sci. Technol. 2 (2013) P515–P523, https://doi.org/10.1149/2.007312jss.

[20] H. Cheng, J. Wu, Q. Yu, H.-J. Kim-Lee, A. Carlson, K.T. Turner, K.-C. Hwang, Y. Huang, J.A. Rogers, An analytical model for shear-enhanced adhesiveless transfer printing, Mech. Res. Commun. 43 (2012) 46–49, https://doi.org/10.1016/j.mechrescom.2012.02.011.